Selection of optimal escape routes in a flood-prone area based on 2D hydrodynamic modelling

Peng Guo[1], Junqiang Xia[1*], Meirong Zhou[1], Roger A. Falconer[2], Qian Chen [1], Xiaolei Zhang[1]

[1] State Key Laboratory of Water Resources and Hydropower Engineering Science, Wuhan University, Wuhan 430072, China.
Email: xiajq@whu.edu.cn

[2] Hydro-environmental Research Centre, School of Engineering, Cardiff University, Cardiff CF243AA, UK

Abstract: Optimizing escape routes during an extreme flood event is an effective way to mitigate casualties by instructing local inhabitants to escape along pre-determined routes. In this study, a model for selecting optimal escape routes in a flood-prone area has been proposed, which includes a module for predicting the two-dimensional (2D) hydrodynamics, and modules for assessing the hazard degree for evacuees, calculation of evacuation times and determination of different escape routes. In the module for determining escape routes, two evacuation schemes were used to determine an optimal escape route, with scheme A developed to find optimal escape routes based on established road networks, and scheme B developed to design a new optimal route for evacuation. Extreme overbank flood events occurred in the Lower Yellow River (LYR) in July 1958 ("58.7") and August 1982 ("82.8") and the proposed model was applied to select the optimal escape routes on the Lankao-Dongming floodplain area of the LYR for these two overbank floods. The corresponding model predictions indicated that the optimal escape routes and the time to evacuate were determined respectively for three starting locations for these two overbank floods. The optimal escape routes for these two floods were the same for all three starting locations, and the optimized routes provided 3h more time for evacuees to escape. The results also showed that the time of evacuation would need to be earlier for the "58.7" overbank flood scenario because of its larger amount of water volume and higher peak discharge.

Key words: hydrodynamic module; human stability; escape speed; escape route; flood-prone area, Lower Yellow River.

1. Introduction

Due to climate change and intensive anthropogenic activity in recent decades, there has been an increasing occurrence in the probability of extreme floods (Milly et al., 2002; Wang et al., 2016). Various kinds of floods, such as overbank and urban floods, continue to be regarded as one of the main sources of casualties for all natural hazards (Niu et al., 2013; Xia et al., 2014; Zhang et al, 2016). According to incomplete statistics, more than 30 overbank flood events have occurred in the Lower Yellow River (LYR) since 1949, with 13,000 villages and 9 million people being affected in total (Niu et al., 2013). There is a large inhabitant population living on floodplains, especially in China, which is the world's most populated country (Piao et al., 2010). Typically when a farm-dike breaches along a floodplain, then rapid flood inundation frequently occurs resulting in a very limited time for issuing warnings, and the inhabitants usually suffer from potential flood risk (Collier, 2007). Therefore, it is desirable to be able to determine optimal escape routes for potential evacuees in terms of flood mitigation for such types of events.

With recent progress in computer-based numerical modelling tools, two-dimensional (2D) hydrodynamic models have been proposed to simulate various processes associated with flood inundation (Liang et al., 2007; Neal et al., 2009; Xia et al., 2010; Liu et al., 2015). These model predictions can present temporal and spatial distributions of the key hydrodynamic parameters for a specific flood scenario, such as flow velocity and water depth. As an important tool for current day flood risk management, such model predictions can be used to assess the flood risk to people and provide the potential to instruct local inhabitants as to when and how to escape. Therefore various evacuation algorithms have been developed for people facing extreme flood events. A Life Safety Model (LSM) developed by BC Hydro in Canada offers a robust method for assessing flood risk associated with the operation of dams or other flood control structures (Johnstone et al., 2005). As a response planning tool, and a means of calculating complex evacuation processes, an evacuation timeline for flood events is an effective procedure, including: flood inundation extent predictions, warning information delivery, and evacuation operation (Stephen et al., 2010). Zhang et al. (2016)

analyzed the distribution of water depth in a flood inundation process using the software MIKE Flood, and proposed a method to extract impassable flooded roads using ArcGIS. Lujak and Giordani (2018) proposed a mathematical model based on two node centrality measures and the model not only predicts the shortest evacuation route, but also considers other relevant characteristics in order to predict the safest evacuation route. Soon et al. (2018) used a semi-parametric estimation approach to obtain the marginal effects of explanatory variables on flood victims' evacuation decisions and analysed the determinants of actual evacuation decisions for an unprecedented 2014 flood disaster. Moshtagh et al. (2018) proposed the stochastic queue core (SQC) model for vehicular evacuation problems, with the average travel time and the operation costs being minimized in the model. These models can be integrated, including a module for predicting the flood inundation extent and a module for evacuation planning, to assess the flood risk for the domain and to provide information for optimal evacuation. However, these models do not consider the stability of victims in floodwaters, and they therefore have limited value in practical decision making for effective flood evacuation response. Previous studies indicate that the stability degree and escape speed of people in floodwaters can influence the safety and time expenditure for evacuation (Abt et al., 1989; Karvonen et al., 2000; Ishigaki et al., 2008; Xia et al., 2014), and these influencing factors need to be considered in the module for selecting optimal escape routes.

Flood risk to people is often estimated empirically according to the magnitude of the water depth, which means that the hazard degree of a human body in floodwater depends solely on the incoming water depth. This method does not take account of the effect of the flow velocity on the stability of a human body, and therefore does not consider the mechanism of people instability in floodwaters. Various criteria for people instability in floodwaters have been proposed. Abt et al. (1989) reported the results of toppling instability experiments of 20 adults, which were conducted in a 61 m long laboratory flume with different ground surfaces. An equation defining the instability threshold of a person in floodwaters was developed using linear regression of the experimental data. Karvonen et al. (2000) undertook stability tests using 7 human bodies on a steel grating platform,

81 towed in a model ship basin, and the product of water depth and velocity was proposed to describe
82 the degree of people stability based on their experimental data. Xia et al. (2014) derived theoretical
83 formulae for the incipient velocity of a human body in floodwaters for the instability modes of
84 toppling and sliding, with more than 50 tests being undertaken for a model human body, with the
85 experimental data being used to calibrate the parameters in the derived mechanics based formulae.
86 Furthermore, Ishigaki et al. (2005) conducted laboratory experiments on the escape speed for
87 people in floodwaters, with the experimental results indicating that the escape speed is closely
88 related to the water depth. Therefore, the degree of stability and escape speed of people in
89 floodwaters needs to be calculated using hydrodynamic parameters, such as water depth and
90 velocity, and any evacuation predictive method would be more practical and reliable if the
91 instability mechanism of evacuees in floodwaters was included in the analysis.

92 In this study, a model for selecting optimal escape routes in flood-prone areas is therefore
93 firstly proposed. Two algorithms have been developed to determine optimal escape routes,
94 including: (i) scheme A – which has been developed to find the optimal escape routes, based on
95 established road networks, and (ii) scheme B – which has been been developed to design a new
96 optimal evacuation route. The 2D hydrodynamic module was then verified against experimental
97 data for flood flows from two physical models of an idealized city (Soares-Frazão and Zech, 2008)
98 and the Toce River (Soares-Frazão and Testa,1999). Finally, the proposed model was then applied to
99 select the optimal escape routes for two overbank flood events occurring on the Lankao-Dongming
100 floodplain (LDF) area of the LYR, with the optimal escape routes and corresponding final escape
101 times being determined.

102

103 **2. Description of an integrated model for** selecting optimal escape routes

104 This section gives details of an existing 2D hydrodynamic module, the modules for assessment
105 of the hazard degree for evacuees, the calculation of the evacuation time and determination of

different escape routes. In general, these modules are integrated as follows: the temporal and spatial distributions of flood parameters, such as flow velocity and water depth, are first provided by the 2D hydrodynamics module. Based on these flood parameters, the hazard degree and escape speed of a potential victim, within a computational cell, are then calculated using the calculation modules for the hazard degree and evacuation time of evacuees. Finally, the optimal escape route and corresponding final escape time can be obtained using the module for the determination of different escape routes. More details are given below.

2.1 2D hydrodynamic module

In order to simulate the flood inundation processes, the depth-integrated 2D shallow water equations are often used to describe flows in natural rivers, floodplain areas and other flood-prone areas, with the equations being written in a general conservative form as follows (Xia et al., 2010a,b):

$$\frac{\partial \boldsymbol{U}}{\partial t}+\frac{\partial \boldsymbol{E}}{\partial x}+\frac{\partial \boldsymbol{G}}{\partial y}=\frac{\partial \tilde{\boldsymbol{E}}}{\partial x}+\frac{\partial \tilde{\boldsymbol{G}}}{\partial y}+\boldsymbol{S} \tag{1}$$

where $\boldsymbol{U}$ = vector of conserved variables; $\boldsymbol{E}$ and $\boldsymbol{G}$ = convective flux vectors for flow in the x and y directions, respectively; $\tilde{\boldsymbol{E}}$ and $\tilde{\boldsymbol{G}}$ = diffusive vectors related to the turbulent stresses in the x and y directions, respectively; and S = source term including: bed friction, bed slope and the Coriolis force. The above terms can be written in detail as:

$$\mathbf{U}=\begin{bmatrix} h \\ hu \\ hv \end{bmatrix},\ \mathbf{E}=\begin{bmatrix} hu \\ hu^2+\frac{1}{2}gh^2 \\ huv \end{bmatrix},\ \mathbf{G}=\begin{bmatrix} hv \\ huv \\ hv^2+\frac{1}{2}gh^2 \end{bmatrix},\ \tilde{\mathbf{E}}=\begin{bmatrix} 0 \\ \tau_{xx} \\ \tau_{yx} \end{bmatrix},\ \tilde{\mathbf{G}}=\begin{bmatrix} 0 \\ \tau_{xy} \\ \tau_{yy} \end{bmatrix} \text{ and } \mathbf{S}=\begin{bmatrix} 0 \\ gh(S_{bx}-S_{fx}) \\ gh(S_{by}-S_{fy}) \end{bmatrix} \tag{2}$$

where u and v = depth-averaged velocities in the x and y directions, respectively; h = water depth; g = gravitational acceleration; S_{bx} and S_{by} = bed slopes in the x and y directions, respectively; S_{fx} and S_{fy} = friction slopes in the x and y directions, respectively; and τ_{xx} τ_{xy}, τ_{yx} and τ_{yy} = components of the turbulent shear stress over the plane.

A cell-centered finite volume method (FVM) was adopted to solve the governing equations, based

on an unstructured triangular mesh. At the interface between two neighboring cells, the calculation of the flow fluxes was treated as a locally one-dimensional problem, thus the flux can be obtained by an approximate Riemann solver. A Roe's approximate Riemann solver, with the scheme of monotone upstream scheme for conservation laws (MUSCL), was employed to evaluate the normal fluxes, and the predictor-corrector procedure was used for time stepping. This approach provided second-order accuracy in both time and space (Tan, 1992). The hydrodynamic module was validated using experimental data from two physical models, with the detailed validation process being given in the following section.

2.2 Assessment of hazard degree of evacuees

Flood risk to people at various sites varies owing to the difference in flood parameters, and it is important to select an appropriate stability criteria for human subjects in flood risk management. Various criteria have been proposed using theoretical and experimental methods (Abt et al., 1989; Karvonen et al., 2000; 2008; Xia et al., 2014). For example, Xia et al. (2014) proposed a mechanics-based formula for the incipient velocity of a human body at toppling instability, and accounted for the effect of body buoyancy and the influence of a non-uniform vertical velocity profile acting on the human body in floodwaters, and this formula is given as:

$$U_c = \alpha\left(\frac{h}{h_p}\right)^{\beta}\sqrt{\frac{m_p}{\rho_f h^2} - \left(\frac{a_1}{h_p^2} + \frac{b_1}{h h_p}\right)(a_2 m_p + b_2)} \tag{3}$$

where U_c= incipient velocity of a human body at toppling instability; ρ_f = density of water; h_p and m_p = height and mass of a human body; a_1 and b_1 = non-dimensional coefficients related to the buoyancy force of a human body, with a_1 = 0.633 and b_1 = 0.367 for a typical human body of a Chinese person; a_2 and b_2 = coefficients determined from the average attributes of a human body, with $a_2 = 1.015\times10^{-3}$ m^3/kg and $b_2 = -4.927\times10^{-3}$ m^3.

Xia et al. (2014) conducted tests in a flume to obtain the water depth and velocity under the condition of toppling instability using a model human body, with the experimental data being used

153 to calibrate two parameters, namely α and β in Eq. (3). **Fig. 1** shows the relationship between the
154 water depth and incipient velocity for a general Chinese adult with a height of 1.71 m and a mass of
155 68.7 kg, with close agreement being obtained between the calculated and measured data. As shown
156 in Figure 1, the incipient velocity for an adult for an incoming depth of 0.5 m is 1.3 m/s.

157 The water depth at a computational cell obtained from the 2D hydrodynamic module is used to
158 calculate the corresponding incipient velocity for a specified adult using Eq. (3), as proposed by Xia
159 et al. (2014). The following relationship is used to quantify the hazard degree, as given by:

160 $$HD = Min\,(1.0,\ U / U_c) \tag{4}$$

161 where HD = hazard degree for a human subject in floodwaters. There are three levels of hazard
162 degree for people in floodwaters according to the value of HD, including: (i) safe ($0 \leqslant HD < 0.6$),
163 (ii) danger ($0.6 \leqslant HD < 0.9$), and (iii) extreme danger ($0.9 \leqslant HD \leqslant 1.0$) (Cox et al., 2010; Xia et
164 al., 2014). This mechanics-based assessment method is more practical and reliable because it
165 accounts for the effects of both water depth and flow velocity.

166 *2.3 Calculation of evacuation time*

167 There exists a time challenge between people evacuation and flood inundation, because these
168 two processes occur concurrently. Therefore, time is regarded as a key factor in an emergent
169 situation during a flood disaster (Pel et al., 2012). The time taken for evacuation is calculated from
170 the escape speed and the corresponding escape distance, which is closely related to the local flow
171 conditions. Ishigaki et al. (2008) conducted evacuation tests in a water tank, for water depths
172 varying from 0.0 m to 0.5 m, with and without a flow velocity of 0.5 m/s. A fitted curve based on
173 the measured speeds of escape on foot and the local water depth is shown in **Fig. 2**. The normal
174 walking speeds of people on dry ground are typically 1.35 and 1.27 m/s for male and female adults,
175 respectively, and the corresponding escape speeds would decrease to 1/2 of the normal walking
176 speed for a typical water depth. However, the transport capacity of a road would also influence the
177 escape speed. An empirical relationship between the water depth and the corresponding escape

speed for people is given by:

$$v_{\mathrm{E}} = \begin{cases} \eta \cdot (1.31 - 3.1h) & (\ h \le 0.2\,\mathrm{m}\ ) \\ \eta \cdot 0.5 v_0 & (0.2 \le h \le 0.8\,\mathrm{m}) \end{cases} \tag{5}$$

where v_0 = normal walking speed of adults; v_{E} = escape speed for people in floodwaters; and η = reduction coefficient of 0.90. Eq. (5) shows that it is difficult for people to escape on foot if h > 0.8 m.

The flow conditions along an escape route would change with time, and each escape route is then divided into several short segments. For a segment between the locations A_i and A_{i+1} at the time t, a time challenge between people escaping and flood inundation is shown in **Figs. 3 and 4**. The flow conditions at A_i at time t are determined based on the 2D hydrodynamic module, which can be used to calculate U_c and HD using Eq. (3) and Eq. (4), respectively. If the value of HD approaches 1.0, namely $U > U_c$, then people in the floodwaters would be in danger; otherwise the escape speed of an evacuee can be calculated using Eq. (5) and then the time to traverse the segment can be determined. The same approach would be used for the next segment until the location of A_{i+1} is one of the safe havens. The total time of travel along all of the segments from A_1 to A_N is given by:

$$t_{\mathrm{N}} = t_0 + \sum_{i=2}^{N} \left[\mathrm{V} L_{\mathrm{i\text{-}1}} / (v_{\mathrm{E,\ i\text{-}1}}) \right] \tag{6}$$

where t_N = time of travel along the segments from A_1 to A_N; t_0 = initial time for evacuees to receive warning; $\triangle L_{\mathrm{i\text{-}1}}$ = length of the i-1 segment between the locations A_{i-1} and A_i, and $v_{\mathrm{E,i\text{-}1}}$ = corresponding escape speed along the i-1 segment.

2.4 Determination of different escape routes

In the proposed model, a selection method of optimal escape routes is presented, comprising schemes A and B, under two scenarios i.e. both with and without the established road networks being considered. These two schemes are described in detail as follows:

(1) For a flood-prone area with completed road networks, the Dijkstra algorithm, which can

find the shortest path between a given source node and a specified destination node, was adopted to determine the shortest routes (Dijkstra, 1959). These routes were taken to be alternative escape routes for scheme A. Then the hazard degree for an evacuee, and the corresponding escape speed for each alternative route, were calculated for a specified flood event. When the hazard degree of the route reached 0.9 for the first time, then this time was defined as the final escape time. The route with the latest final escape time was selected as the optimal escape route.

(2) For a flood-prone area with uncompleted road networks, a location was defined as the temporary safe haven if the value of *HD* for an evacuee is less than 0.6. These locations were zoned by the temporal and spatial distributions of the hydrodynamic parameters for different flood frequency occurrences. For a starting location in the flood-prone area, the corresponding shortest route was selected as an optimal escape route to safe havens for scheme B. These routes would provide a reference for the construction of new roads, which would be useful for both transportation and evacuation.

In these two schemes, optimal escape routes and corresponding final escape times can be obtained, which provide a scientific basis for planning evacuation. However, these methods are based more on the mechanics-based instability and escape speed of evacuees, and cannot account for the complicated effects of age, gender and educational level of evacuees.

3. Verification of the hydrodynamic module

In order to estimate the escape speed and corresponding flood risk to people predicting, or modelling, the flood inundation extent is the most important precondition. Therefore, the hydrodynamic module presented above was first verified against experimental data of flood flows based on data from two physical model studies, including: (i) an idealized city (Soares-Frazão and Zech, 2008) and (ii) the Toce River (Soares-Frazão and Testa,1999). These results show that the hydrodynamic module can accurately predict various hydrodynamic parameters factors. The details of the model tests are given in this section.

226 *3.1 Flood propagation through an idealized city*

227 Experiment of flood flow through an idealized city were conducted in a 36×3.6 m flume
228 located in the civil engineering laboratory of the Université Catholique de Louvain, Belgium
229 (Soares-Frazão and Zech, 2008), with a sketch map of the initial set-up being shown in **Fig. 5**. A
230 gate between the reservoir and downstream was located at x = 0 m, and the initial depths were 0.400
231 m and 0.011 m for the reservoir and downstream, respectively. The sketched city was idealized
232 using 5×5 buildings, which were high enough so that they were not submerged by floodwaters, with
233 the buildings being 0.3×0.3 m and with each street being 0.1 m.

234 In the test case, the study domain was divided into 23,346 unstructured triangular cells and the
235 mesh was refined around each building with an area of about 2 cm^2. A free-slip boundary condition
236 was applied at the walls, and a free outflow boundary condition was used at the downstream outlet.
237 A Manning roughness value of 0.010 $m^{-1/3}s$ (Soares-Frazão and Zech, 2008), a minimum water
238 depth value of 0.001 m and a time step of 0.0001 s were set to simulate the flood inundation
239 processes occurring, following the opening of the gate.

240 **Fig. 6** shows the water level profiles along the longitudinal street at y=0.2 m at 5 s and 10 s. It
241 can be seen that the calculated water depth profiles were in close agreement with the measured
242 profiles, with correlation coefficients of R^2=0.88 and 0.82 at 5 s and 10 s, respectively. However,
243 the calculated depth-averaged velocity profiles were not in such close agreement with the measured
244 data, with correlation coefficients of R^2=0.71 and 0.75 at the respective times. In most cases the
245 measured water-surface velocities (Soares-Frazão and Zech, 2008) were slightly higher than the
246 calculated depth-averaged velocities. This test case therefore indicates that the 2D hydrodynamic
247 module can generally present a credible prediction of the hydrodynamic parameters for flooding in
248 a scaled model environment.

249 *3.2 Flood propagation in the Toce River.*

250 A physical model of the Toce River was built at ENEL HYDRO laboratories in Milan, Italy,

consisting of a 1:100 scaled replication of almost 5 km of the river. As shown in **Fig. 7**, a large reservoir was located in the central part of the model, and a set of water probes were located at various points across the model to record the variation in elevations with time (Soares-Frazão and Testa,1999).

In the test case, the study domain was divided into 21,396 unstructured triangular cells and the mesh was locally refined around the upstream and downstream boundaries and near the reservoir, with the minimum and maximum cell areas being 10 cm^2 and 736 cm^2, respectively. The initial water depth was set to 0.001 m for the dry bed of the domain and a free outflow boundary condition was applied at the downstream outlet. A constant time step of $\Delta t = 0.001$ s and constant Manning's roughness coefficient of $n = 0.0162$ $m^{-1/3}s$ (Soares-Frazão and Testa, 1999) were adopted in the module. In addition, the minimum water depth for treating the wetting and drying fronts was set to 0.001 m for this study.

Fig. 8 shows the variation in the measured and calculated water levels at the sites P_1, P_4, P_{13} and P_{19}. It can be seen that the calculated depths were in close agreement with the measured values, with correlation coefficients of $R^2 = 0.84$, 0.75, 0.70 and 0.88, respectively. It was concluded from these comparisons that the 2D hydrodynamic module was accurately predicting the hydrodynamic parameters in a flood-prone area with complex topography.

4. Model application

4.1 Study area

In order to determine optimal escape routes in the LDF, related measurements were collected from the YRCC (Yellow River Conservancy Committee), including: topography, surface landforms, overbank floods occurring in the Dongming floodplain area, and discharge hydrographs at Jiahetan for 1958 and 1982. In total there are about 120 natural floodplain areas in the LYR, which are inhabited by 1.9 million residents, with overbank flood events only occurring on the LDF area during flood seasons. In particular, there was also a serious flood on the LDF area in 2003 due to a

276 farm-dike breach, with 114 villages and 12,000 hm^2 of farmland being submerged, and with
277 160,000 people being affected. Therefore, it is important for people living on flood-prone areas to
278 be able to escape efficiently in emergency situations. In this study two extreme overbank floods
279 occurred on the LDF area in July 1958 and August 1982, with the corresponding peak discharges
280 being 20,500 and 14,500 m^3/s respectively, at the hydrometric station of Jiahetan (**Fig. 9**). The
281 proposed model was applied to select optimal escape routes for these two overbank flood events,
282 assuming that the discharge hydrograph entering the floodplain zone for each flood scenario was
283 equivalent to the hydrograph at Jiahetan, minus the current bank-full discharge (7,000 m^3/s) along
284 this reach. The locations of a flood diversion sluice, three starting locations (SL_{1-3}), two observation
285 points (P_1 and P_2) and target safety areas are shown in **Fig. 9**. The flood inundation extent on the
286 LDF area during the "82.8" flood are given in detail. Comparisons of the locations and final escape
287 times for optimal escape routes are presented for the "58.7" and "82.8" flood events.

288 *4.2 Simulation of "82.8" overbank flood*

289 The study domain covered an area of about 250 km^2 and was divided into 16,064 unstructured
290 triangular cells, which included a significant slope in the southeast direction of the LDF area (**Fig.**
291 **10**). The simulations included: a constant time step of 0.2 s, and a constant Manning roughness
292 coefficient of 0.060 $m^{-1/3}s$ for village areas and 0.035 $m^{-1/3}s$ for other underlying surfaces (Zhang et
293 al., 2016).

294 As shown in **Fig. 11**, the corresponding water depth was 1.2 m when the hazard degree for
295 people at P_1 reached 1.0 at t=10.9 h; however, the corresponding water depth was 1.4 m when the
296 hazard degree for people at P_2 was equal to 1.0 at t=35.6 h. The location of P_1 was near the flood
297 diversion sluice, with the local velocity being higher than that at P_2. Thus, it is more reliable to
298 evaluate human stability using Eq. (3) and Eq. (4), because people would be swept away under the
299 condition of small water depth and large flow velocity.

300 In addition, the hazard degree distributions for people at t=9, 13 and 33 h are shown in **Fig. 12**.
301 It can be seen that the area including the dangerous zone would increase gradually along the levee

due to the relatively large slope in the southeast direction on the LDF area. All the inhabitants would be in danger at t=49 h, and they would have to escape according to the optimal route.

4.3 Determination of optimal escape routes in the "82.8" overbank flood

(a) Optimal escape routes for scheme A

The optimal escape routes for scheme A are presented for three starting locations. As shown in **Fig. 9**, and using the Dijkstra algorithm, 5 alternative routes for each starting location are presented, with the optimal escape routes for scheme A being selected. The variation in the hazard degree for evacuees along the optimal routes and the worst routes for the three starting locations are shown in **Fig. 13**. The duration was only about 1.5 h when the *HD* value increased from 0.0 to 1.0 for each escape route. However, the evacuees at SL_1 would be eventually rescued if they selected the worst route S_1 to escape and were aware of the danger before t=5.9 h, as the *HD* value was equal to 0.9. Similarly, they would be eventually rescued if they were aware of the danger and selected the optimal route S_5 to escape before t=10.7 h. Therefore, the route S_5 was selected as the optimal route for SL_1, with the corresponding final escape time being t=10.7 h. In a similar manner, the route S_9 was selected as the optimal route for SL_2, with the corresponding final escape moment of t=11.7 h; and the route S_{13} was selected as the optimal route for SL_3, with the corresponding final escape time being t=14.7 h.

(b) Optimal escape routes for scheme B

People need to escape at SL_1, SL_2 and SL_3, since they would be in danger if they were not aware of warnings before t=19.9, 20.7 and 22.2 h regards. The optimal escape routes for scheme B are presented in **Fig. 9,** with the corresponding final escape times being given in **Table 1**. For example, the period from the time when people started to escape at t=19.9 h increased gradually, and the temporary safe haven would border on the target safe haven at S_1 for the first time after a period of 6.7 h. Thus, the final escape time would be t =13.2 h if evacuees chose the route SL_1-S_1. In a similar way, the final escape times were t==16.6 h and 17.5 h if escapees selected the routes SL_2-S_2 and SL_3-S_3.

A comparison of the final escape times between schemes A and B is shown in **Table. 1**. As compared with the optimal routes for scheme B, the time for inhabitants to evacuate based on the optimal times for scheme A were 2.5, 4.9 and 2.8 h respectively for the three routes considered. The optimal route SL_2-S_2 was close to the route SL_2-S_9, and the optimal route SL_3-S_3 was also close to SL_3-S_{13}. The results provide evidence for adjusting the existing routes slightly. However, the optimal route SL_1-$S_{1'}$ was very different from the route SL_1-S_5. Thus, for a flood-prone area with an incomplete road network, the construction of new routes can be considered based on the current calculation results, since the routes would be useful for evacuation and transportation.

4.4 Optimal escape routes for the "58.7" overbank flood event

The optimal escape routes and corresponding final escape times were also calculated for the "58.7" overbank flood event, with the results for schemes A and B being shown in **Table 1**. The optimal escape routes were the same for these two overbank floods, both for schemes A and B, but the corresponding final escape times for scheme A for the "58.7" flood event were 1-3 h earlier than those for the "82.8" flood, and the final escape times for scheme B for the "58.7" flood event were about 3 h earlier than those for the "82.8" flood event. A comparison of these results indicates that the optimal escape routes for the 3 starting locations could be determined, but the corresponding final escape times for the "58.7" flood were earlier since the peak discharge and water volume for the "58.7" flood event were greater than those for the "82.8" flood event. These results mean that the escape routes would be the same for floods with different occurrence frequencies, but the final escape times should be calculated based on the model predictions of flood inundation extent processes.

5. Conclusions

In the current study, an integrated numerical model has been developed to select optimal escape routes in flood-prone areas, with the model including: a module for predicting the 2D hydrodynamics, and additional modules for assessing the: hazard degree for evacuees, the

calculation of evacuation times and the determination of different escape routes. The conclusions obtained from this study can be summarized as follows:

(i) A 2D hydrodynamic module was used to simulate the flood inundation extent and processes over a flood-prone area. A detailed validation process was undertaken of the model, which showed that the hydrodynamic module was capable of predicting the hydrodynamic parameters over complex urban and rural topographies. The mechanics-based formula for the incipient velocity of a human body at toppling instability was adopted to assess the stability degree of evacuees in floodwaters. An empirical relationship between the water depth and corresponding escape speed was used to calculate the cumulative time required for evacuation. The selection method of optimal escape routes was presented, comprising schemes A and B, and for scenarios with and without established road networks being considered.

(ii) Model application to the LDF area showed that: optimal escape routes and corresponding final escape times were determined for three starting locations, for schemes A and B, for the "58.7" overbank flood event, which would provide about 3 h and 5 h more for issuing warnings and evacuation procedures, as compared to the worst case escape routes. The optimal escape routes for the "82.8" and "58.7" overbank flood events were the same as for the previous three starting locations. However, the final escape time for the "58.7" overbank flood event would be earlier since there was a larger water volume and a higher peak discharge.

Acknowledgements

The study was partly supported by the National Natural Science Foundation of China (Grant Nos. 51725902 and 51579186), and the Key Cultivating Project from Wuhan University (Grant No. 2042017kf0238). It was also partly supported by two international projects of the Global Challenges Research Fund at Cardiff University and the UK-China Urban Flooding Research Impact Programme.

References

[1] Abt, S. R., Wittler, R. J., Taylor, A. & Love, D. J. 1989 Human stability in a high flood hazard. Water Resources Bulletin 25 (4): 881-890.

[2] Cheng, C., Qian, X., Zhang, Y., Wang, Q. & Sheng, J. 2011 Estimation of the evacuation clearance time based on dam-break simulation of the Huaxi dam in Southwestern China. Natural Hazards 57: 227-243.

[3] Collier, C. G. 2007 Flash flood forecasting: what are the limits of predictability?, Quarterly Journal of the Royal Meteorological Society 133: 3-23.

[4] Cox, R. J., Shand, T. D. & Blacka, M. J. 2010 Australian Rainfall and Runoff: Appropriate Safety Criteria for People. Engineers Australia, Barton, ACT, Australia, Report P10/S1/006.

[5] Dijkstra E. W (1959) A note on two problems in connexion with graphs. Numerische Mathematik, 269-271.

[6] He, X. Y., Wang, Z. Y. & Huang, J. C. 2008 Temporal and spatial distribution of dam-failure events in China. International Journal of Sediment Research 23: 398-405.

[7] Huang X. 2017 The decision method of emergency supplies collection. Natural Hazards 85: 869-886.

[8] Ishigaki, T., Kawanaka, R., Onishi, Y., Shimada, H., Toda, K. & Baba, Y. 2008 Assessment of safety on evacuating route during underground flooding. Proceedings of 16th IAHR-APD Congress and 3rd Symposium of IAHR-ISHS. Nanjing, China, pp. 141-146.

[9] Johnstone, W. M., Sakamoto, D., Assaf, H. & Bourban, S. 2005 Architecture, Modelling Framework and Validation of BC Hydro's Virtual Reality Life Safety Model. International Symposium on Stochastic Hydraulics, Nijmegen, The Netherlands, pp. 23-24.

[10] Karvonen, R.A., Hepojoki, H.K., Huhta, H.K. & Louhio, A. 2000 The use of physical models in dam-break analysis. RESCDAM Final Report. Helsinki University of Technology, Helsinki, Finland, PP. 57.

[11] Liang, D. F., Lin, B. L. & Falconer, R. A. 2007 A boundary-fitted numerical model for flood routing with shock-capturing capability. Journal of Hydrology 332, 477-486.

[12] Liu, Q., Qin, Y., Zhang, Y. & Li, Z. W. 2015 A coupled 1D-2D hydrodynamic model for flood simulation in flood detention basin. Natural Hazards 75: 1303-1325.

[13] Lujak M. & Giordani S. 2018 Centrality measures for evacuation: Finding agile evacuation routes, Future Generation Computer Systems 83: 401–412.

[14] Milly, P. C. D., Wetherald, R. T., Dunne, K. A. & Delworth, T. L. 2002 Increasing risk of great foods in a changing climate. Nature 415: 514-517

[15] Moshtagh M., Fathali J. & Smith M. J., 2018 The Stochastic Queue Core problem, evacuation networks, and state-dependent queues, European Journal of Operational Research 269: 730–748.

[16] Mozumder, P. & Va´squez, W. F. 2015 An empirical analysis of hurricane evacuation expenditures. Natural Hazards 79: 81–92

[17] Neal, J., Fewtrell, T. & Trigg, M. 2009 Parallelisation of storage cell flood models using OpenMP. Environmental Modelling & Software 24(7): 872-877.

[18] Niu, Y. G., Danmu, L. M., Geng, M. Q. & Li, Y. Q. 2013 Discussion on zoned harnessing of the lower Yellow River floodplain. Yellow River, 2013, 35(1): 7-9, 13. (in Chinese).

[19] Piao, S. L., Ciais, P., Huang, Y., Shen, Z. H., Peng, S. S., Li, J. S., Zhou, L. P., Liu, H. Y., Ma, Y. C., Ding, Y. H, Friedlingstein, P., Liu, C. Z., Tan, K., Yu, Y. Q., Zhang, T. Y. & Fang, J. Y. 2010 The impacts of climate change on water resources and agriculture in China. Nature 467: 43-51.

[20] Pel, A. J., Bliemer, M. C. & Hoogendoorn, S. P. 2012. A review on travel behavior modelling in dynamic

traffic simulation models for evacuations. Transportation 39: 97–123

[21] Soares-Frazão, S. & Testa, G. 1999 3rd CADAM meeting - The Toce River test case: Numerical results analysis.

[22] Soares-Frazão, S. & Zech, Y. 2008 Dam-Break flow through an idealized city. Journal of Hydraulic Research, 46(5): 648-658.

[23] Soon, J. J., Kamaruddin R. & Anuar A. R. 2018 Flood victims' evacuation decisions: a semi-nonparametric estimation, International Journal of Emergency Services 7(2):134-146.

[24] Stephen, O., Peter, C. O. & Belinda, D. 2010 Timeline modelling of flood evacuation operations. Procedia Engineering 3: 175-187.

[25] Tan. W. Y. 1992 Shallow Water Hydrodynamics: Mathematical Theory and Numerical Solution for a Two-Dimensional System of Shallow Water Equations. Elsevier, New York.

[26] Van Leer, B. 1979 Towards the ultimate conservative difference scheme. V. A. second order sequel to Godunov's method. Journal of Computational Physics 32: 101-136.

[27] Wang, G. Q., Xia, J. Q. & Wu, B. S. 2008 Numerical simulation of longitudinal and lateral channel deformations in the braided reach of the Lower Yellow River. Journal of Hydraulic Engineering 134(8): 1064-1078.

[28] Wang, K., Wang, L., Wei, Y. M. & Ye, M. S. 2013 Beijing storm of July 21, 2012: observations and reflections. Natural Hazards 67(2): 969-974.

[29] Xia, J. Q., Falconer, R. A., Wang, Y. J. & Xiao, X. W. 2014 New criterion for the stability of a human body in floodwater. Journal of Hydraulic Research 53(4): 93-104.

[30] Xia, J. Q., Falconer, R. A., Lin, B. L. & Tan, G. M. 2010a Modelling dam-break flows over mobile beds using a 2D coupled approach, Advances in Water Resources 33:171–183

[31] Xia, J. Q., Falconer, R. A., Lin, B. L. & Tan, G. M. 2010b Modelling floods routing on initially dry beds with the refined treatment of wetting and drying, International Journal of River Basin Management 8(3-4): 225-243.

[32] Zhang, W. 2016 Emergency evacuation planning against dike-break flood a GIS-based DSS for flood detention basin of Jingjiang in central China. Natural Hazards 81: 1283–1301

[33] Zhang, X. L., Xia, J. Q. & Li, N. 2016 Impacts of mesh scale and village region roughness on predictions of flood inundation over complex floodplains. Journal of Hydroelectric Engineering. 35(10): 48-57 (in Chinese).

Table 1 Optimal escape routes and corresponding final escape times for the "58.7" and "82.8" overbank flood events

Floods		Scheme A			Scheme B		
"82.8"	Optimal escape routes	SL_1~S_5	SL_2~S_9	SL_3~S_{13}	SL_1~$S_{1'}$	SL_2~$S_{2'}$	SL_3~$S_{3'}$
	Final escape moments (h)	10.7	11.7	14.7	13.2	16.6	17.5
"58.7"	Optimal escape routes	SL_1~S_5	SL_2~S_9	SL_3~S_{13}	SL_1~$S_{1'}$	SL_2~$S_{2'}$	SL_3~$S_{3'}$
	Final escape moments (h)	8.4	10.2	13.2	10.5	13.4	14.9

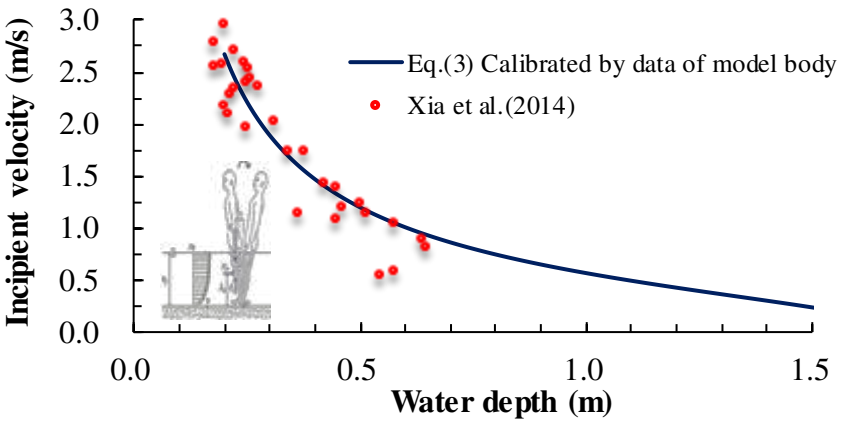

Figure 1. Instability curves between water depth and incipient velocity for Chinese adults in floodwaters

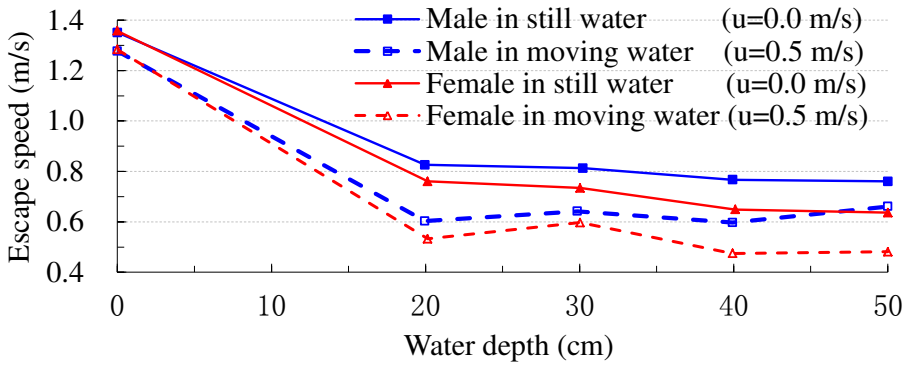

Figure 2. Empirical curves related to the water depths and corresponding escape speeds for adults in floodwaters (From Ishigaki et al., 2008)

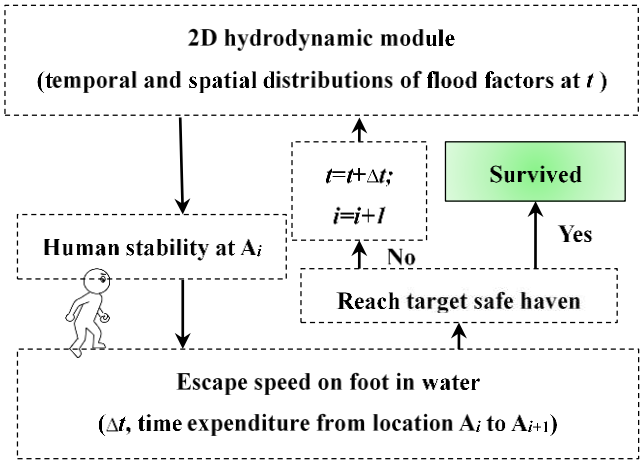

Figure 3. Time competition between people evacuation and flood inundation

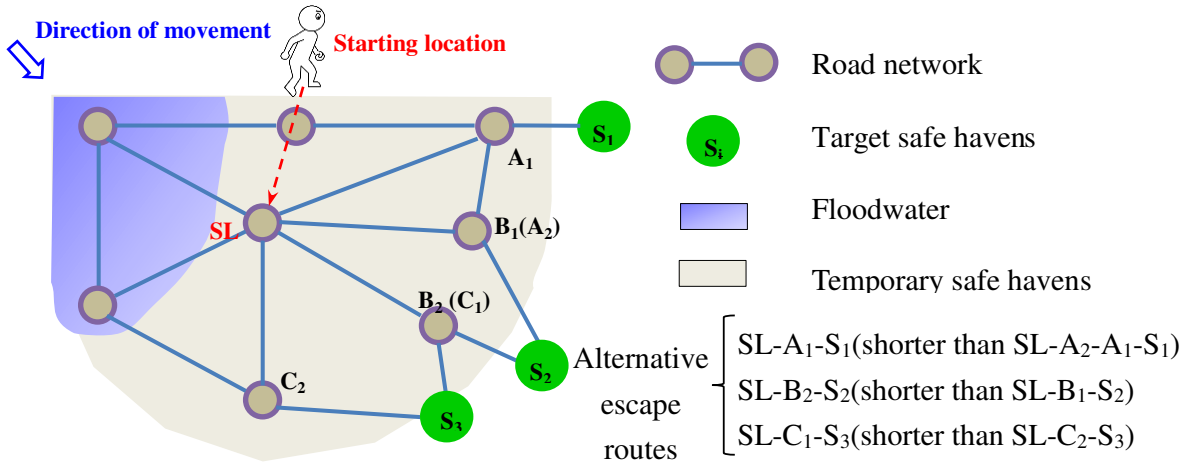

Figure 4. Sketch diagram for an evacuee to escape in a flood-prone area

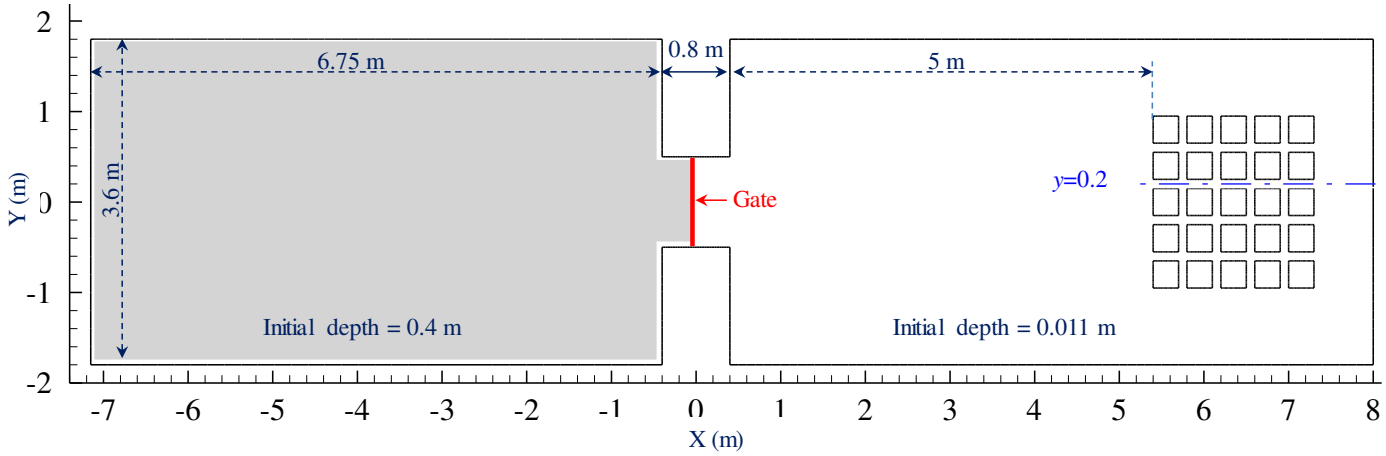

Figure. 5 Sketch of an idealized city in a laboratory flume 虚线

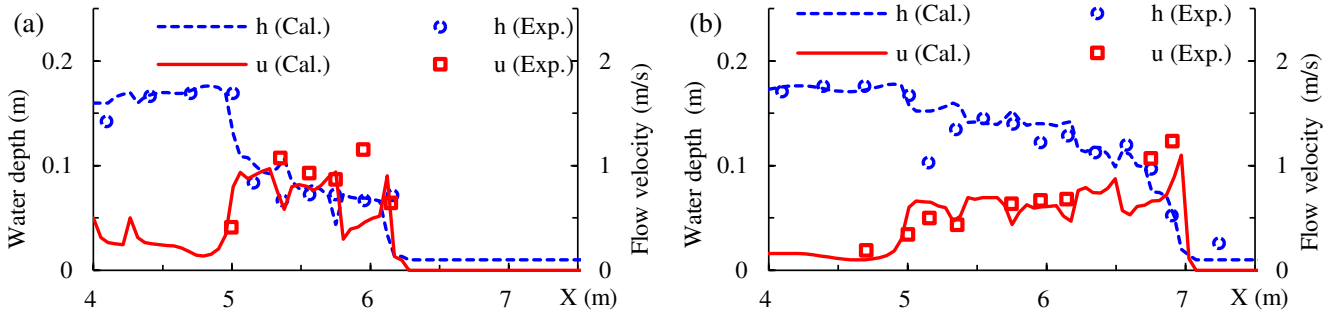

Figure. 6 Comparisons between the calculated and measured water depths and velocities along the longitudinal street at different times: (a) *t*=5 s and (b) *t*=10 s

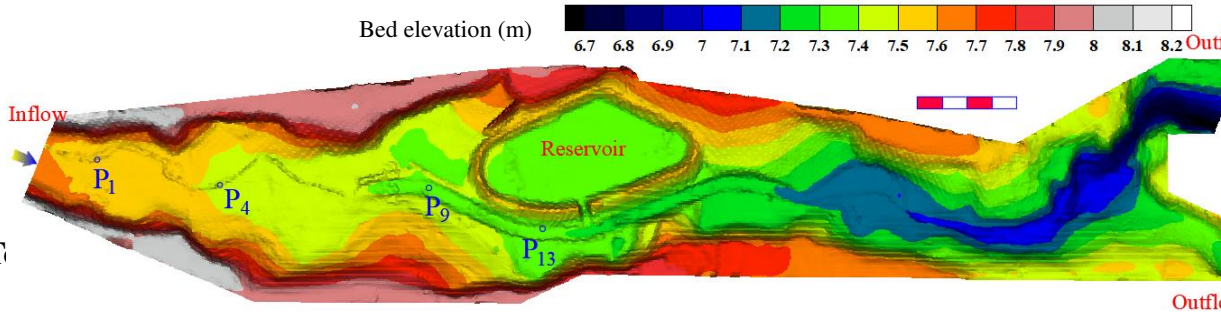

Figure 7. T

monitoring points

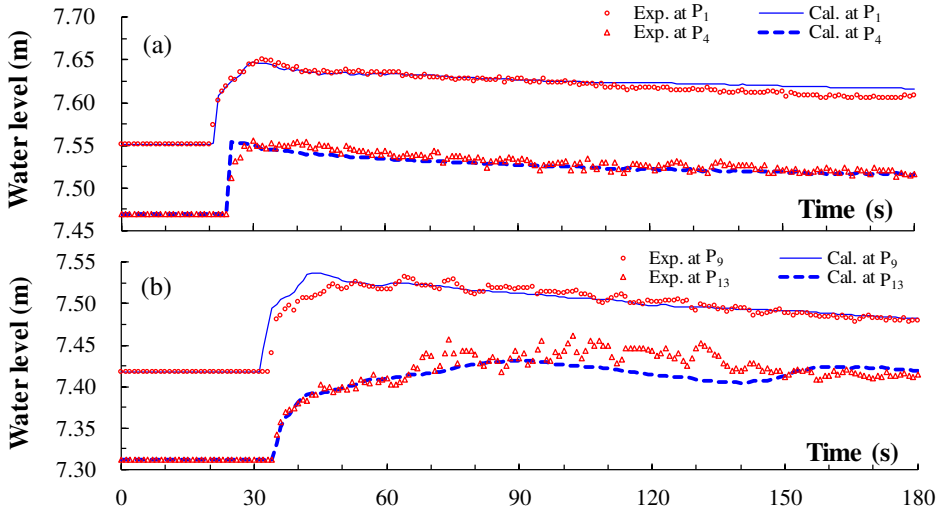

Figure 8. Comparisons between the calculated and measured water levels at different monitoring points: (a) P_1 and P_4; and (b) P_9 and P_{13}.

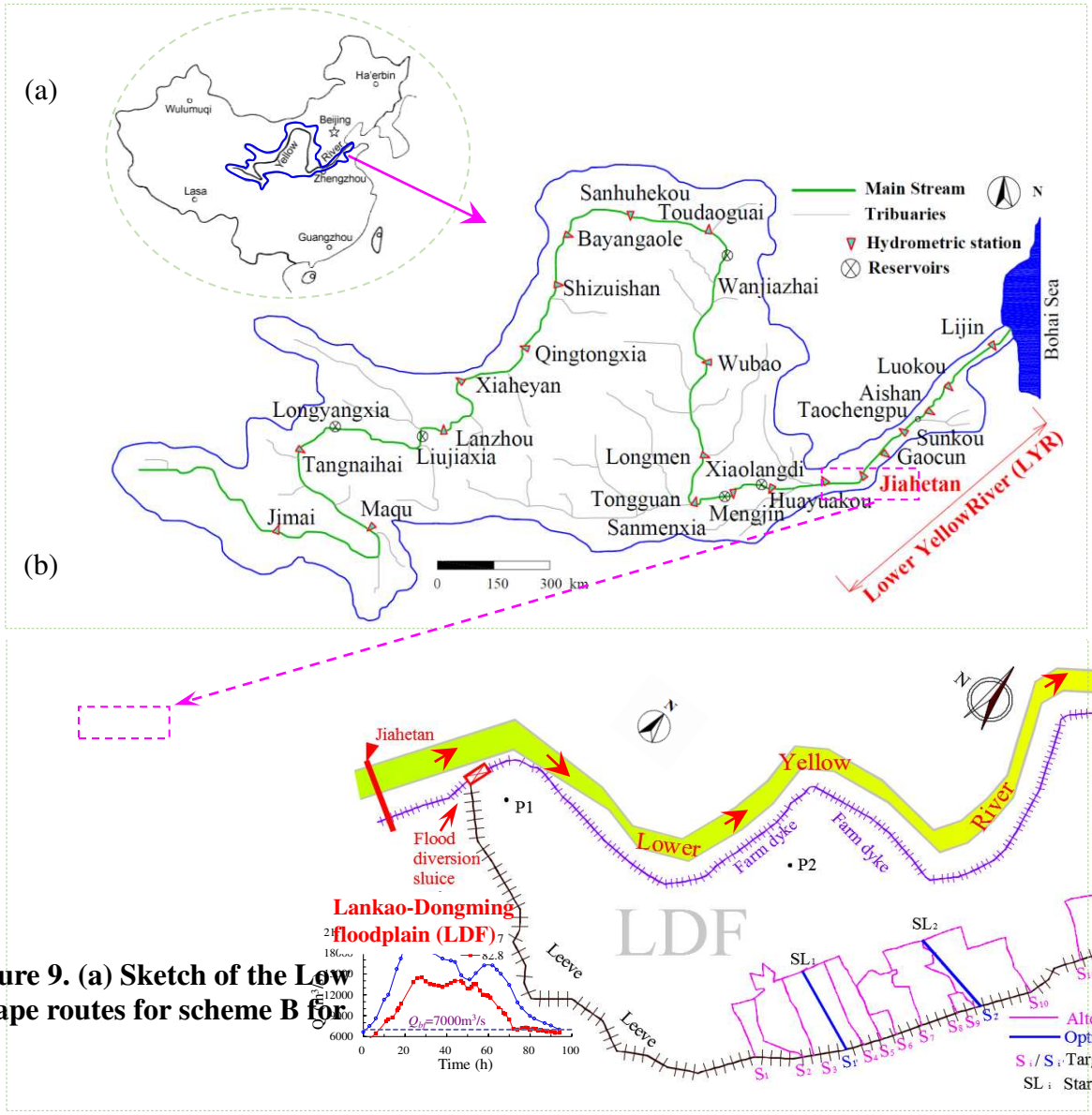

Figure 9. (a) Sketch of the Low
escape routes for scheme B for

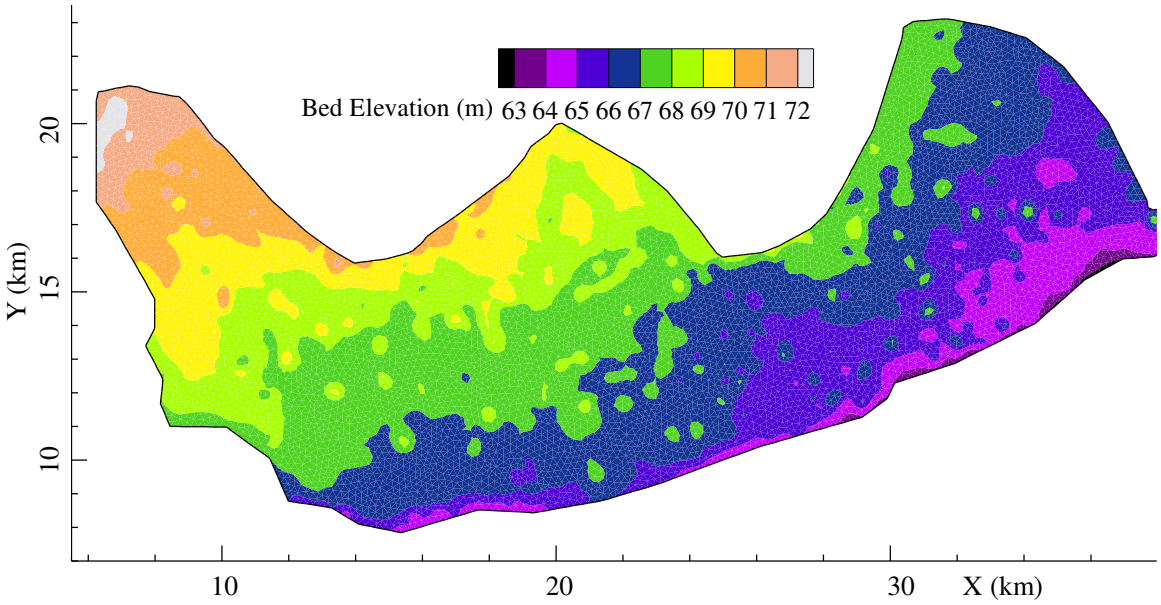

Figure 10. Topography of the study domain

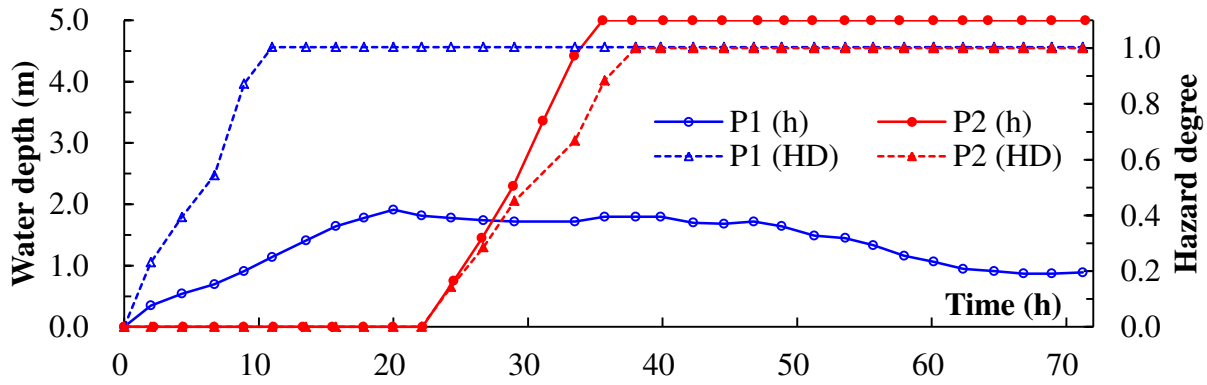

Figure 11. Temporal variations in water depth and hazard degree for people at different points P1 and P2

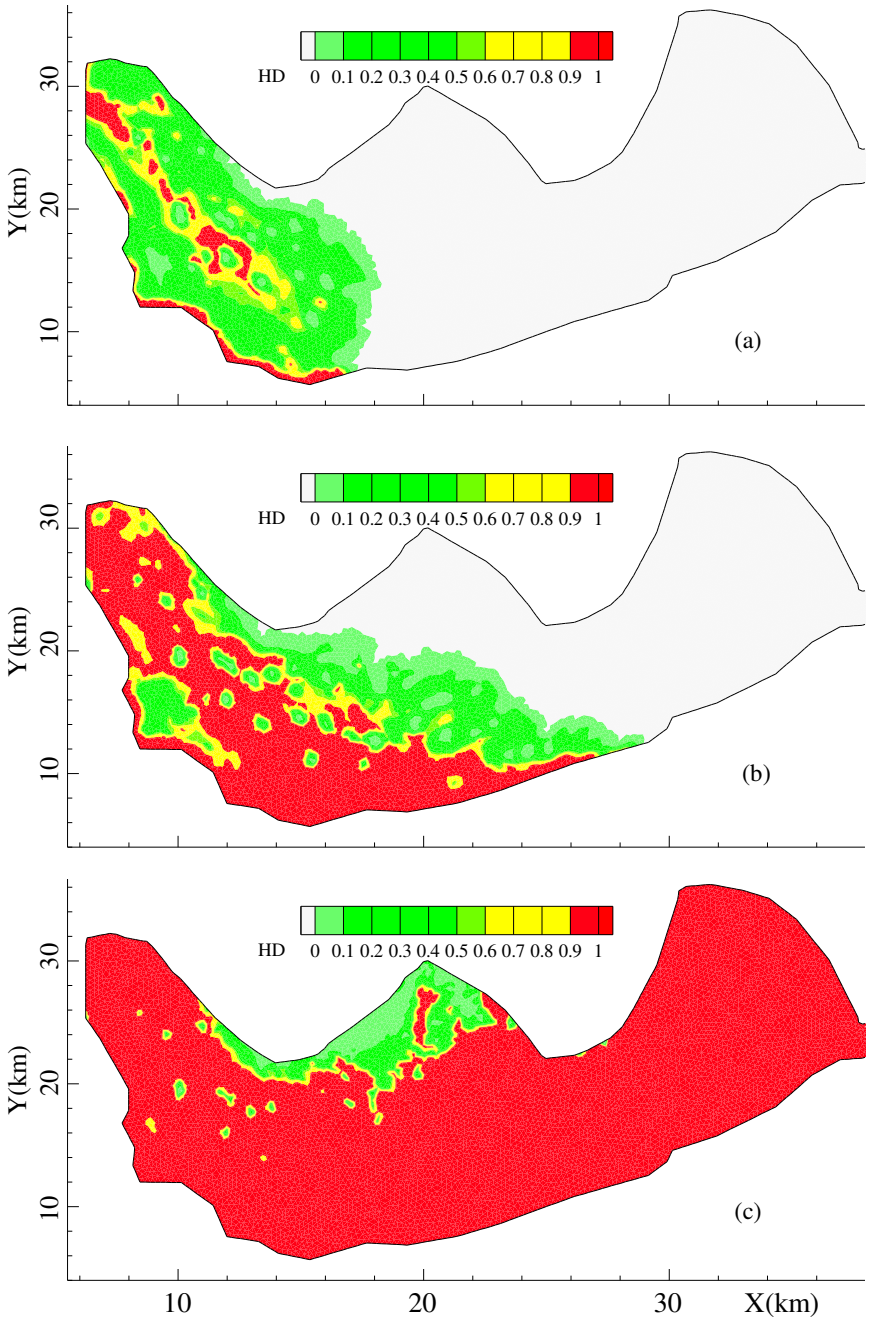

Figure 12. Distributions of hazard degree for people at different times: (a) t=9h, (b) t=13h and (c) t=33h

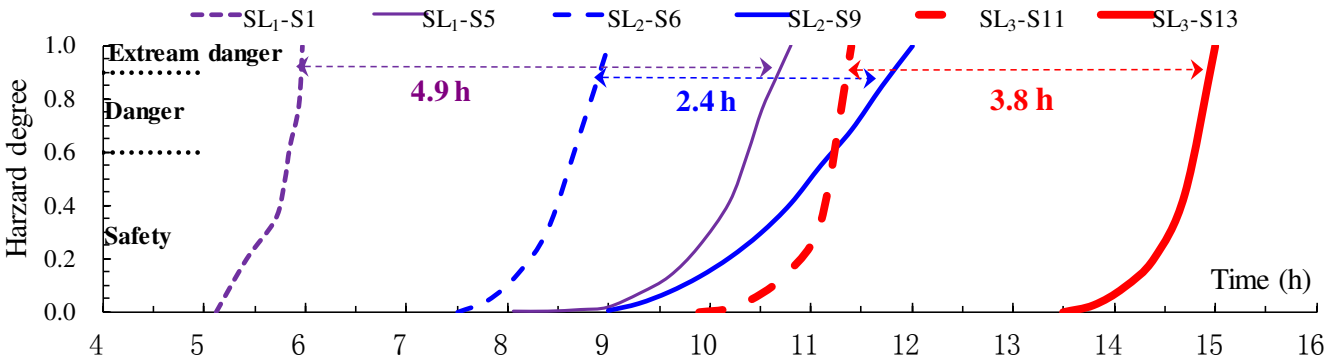

Figure 13. Temporal variations in hazard degree for people using alternative routes